On the Invariant Distribution of Galaxies in the $\mathrm{r_e} - <\mu>_\mathrm{e}$ plane out to $\mathrm{z} = 0.64$[1]

F. La Barbera, G. Busarello, P. Merluzzi, M. Massarotti

and

M. Capaccioli

labarber@na.astro.it

INAF Osservatorio Astronomico di Capodimonte, Napoli, Italy

ABSTRACT

We study the evolution of the relation between half-light (effective) radius, $\mathrm{r_e}$, and mean surface brightness, $<\mu>_\mathrm{e}$, known as Kormendy relation, out to redshift $\mathrm{z} = 0.64$ in V-band restframe on the basis of a large sample of spheroidal galaxies ($\mathrm{N} = 228$) belonging to three clusters of galaxies. The present sample constitutes the largest data set for which the Kormendy relation is investigated up to a look-back time of ~ 6 Gyr ($\mathrm{H_0} = 70\ \mathrm{Kms^{-1}Mpc^{-1}}, \Omega_\mathrm{M} = 0.3, \Omega_\Lambda = 0.7$). A new fitting procedure, which suitably accounts for selection criteria effects, allows for the first time to study the trend of the slope (β) and of the intrinsic dispersion ($\sigma^{(\mathrm{i})}_{<\mu>_\mathrm{e}}$) of the Kormendy relation, and the properties of the whole distribution in the $\mathrm{r_e} - <\mu>_\mathrm{e}$ plane as a function of look-back time. The slope β of the relation does not change from $\mathrm{z} = 0.64$ to the present epoch: $\beta = 2.92 \pm 0.08$, implying a tight constraint of 18–28% on the variation of the stellar formation epoch along the sequence of spheroidal galaxies per decade of radius. The intrinsic dispersion of the relation, $\sigma^{(\mathrm{i})}_{<\mu>_\mathrm{e}} = 0.40 \pm 0.03$, does not vary with redshift and the distribution of galaxy sizes as well as the distribution in the plane of the effective parameters do not vary among the clusters, as proven by the Kolmogorov–Smirnov tests. We conclude that, whatever the mechanism driving galaxy evolution is, it does not affect significantly the properties of bright galaxies in the $\log \mathrm{r_e} - <\mu>_\mathrm{e}$ plane at least since $\mathrm{z} = 0.64$. The evolution of the zeropoint of the Kormendy relation is fully explained by the cosmological dimming in an expanding universe plus the passive luminosity evolution of stellar populations with high formation redshift ($\mathrm{z_f} > 2$).

Subject headings: Galaxies: evolution – Galaxies: fundamental parameters (effective radii, mean surface brightness) – Galaxies: clusters: individual: A 209, AC 118, EIS 0048 – Galaxies: statistics – Galaxies: photometry

1. Introduction

Early–type galaxies (ETGs) are known to populate a two-dimensional manifold in the space of their observed quantities. This Fundamental Plane (FP) is usually expressed by a correlation among the effective radius r_e, the mean surface brightness $<\mu>_e$ within r_e, and the central velocity dispersion σ_0:

$$\log r_e = a \cdot \log \sigma_0 + b \cdot <\mu>_e + c. \tag{1}$$

Due to the small intrinsic dispersion ($\sim 10\%$ in r_e and σ_0, and ~ 0.1 mag in $<\mu>_e$), the FP is considered as a powerful tool to measure galaxy distances and to constrain the processes driving galaxy evolution (e.g. Kjærgaard, Jørgensen, and Moles 1993; Jørgensen, Franx, and Kjærgaard 1996; Jørgensen et al. 1999; Kelson et al. 2000).

A relevant projection of the FP is the correlation between R_e and $<\mu>_e$, also known as Kormendy relation (hereafter KR):

$$<\mu>_e = \alpha + \beta \cdot \log R_e, \tag{2}$$

where R_e is the effective radius in kpc, and $\beta \simeq 3$ (Kormendy 1977). Different studies have demonstrated that in the nearby universe bright ETGs define a sharp sequence in the $\log R_e$–$<\mu>_e$ plane, with an intrinsic dispersion of $\sim 0.3 - 0.4$ in $<\mu>_e$ (Hamabe and Kormendy 1987; Hoessel, Oegerle, and Schneider 1987; Sandage and Perelmuter 1991; Sandage and Lubin 2001). Moreover, Capaccioli, Caon, and D'Onofrio (1992) have shown that ETGs + bulges form two distinct families in the plane of the effective parameters: that of the bright ETGs, following the KR, and another 'ordinary' family, whose properties are more disperse and heterogeneous. Recently, Graham and Guzmàn (2003, see also references therein) demonstrated that the claimed dichotomy between the bright and the dwarf ETGs is only apparent and that there is a continuous structural relation between the two classes. In particular, the different behavior of bright and dwarf ETGs in the $\log R_e$–$<\mu>_e$ plane, and the change in slope of their relations, do not imply a different formation mechanism but can be interpreted with systematic changes in the profile shape with galaxy magnitude.

In order to understand the processes underlying galaxy formation and evolution, it is crucial to investigate the FP and the other relations between galaxy parameters at different look-back times. In the monolithic formation scenario (Larson 1974), ETGs form at very high redshifts in a strong burst of star formation, and the distribution of galaxies in the space of observed quantities changes with redshift due to the passive fading of their stars. In the

---

[1]Based on observations collected at European Southern Observatory

hierarchical framework, bright ETGs form by the progressive merging of smaller units, and the FP relations are built up with redshift. Different works have shown (1) that (dissipationless) merging seems to move galaxies along the FP (Capelato, de Carvalho, and Carlberg 1995; Dantas et al. 2002), and (2) that in hierarchical models, the luminosity–weighted ages of stellar populations in cluster galaxies appear to be the same of those predicted for pure passive evolution (e.g. Kauffmann 1996). All these facts suggest that for both scenarios dynamical effects could play a minor role in the evolution of scaling correlations. It is expected that the FP slopes change with redshift mainly for possible differences in properties of galaxy stellar populations (such as age and metallicity) along the early-type sequence, while the zero point varies consistently with the evolution of a passive stellar population. In the hierarchical framework, however, it is also expected that the distribution in the space of observed quantities evolves with redshift, as merging proceeds to larger and larger sizes. Clearly, in order to analyze this subject, large samples of galaxies are needed at different look-back times.

In the recent years, it has become feasible to study the scaling relations at intermediate redshifts. Due to the heavy demand of observing time in velocity dispersion measurements, many studies have investigated pure photometric laws, like the KR. The main effort to constrain the evolution of the KR slope with redshift has been performed by Ziegler et al. (1999), who analyzed ETGs properties in four clusters at $z \sim 0.4$ and in one at $z = 0.55$, with an average of $\sim$ 20–30 galaxies per cluster. These authors found that the slope is comprised between 2.2 and 3.5 both for the Coma and for the distant clusters, depending on the selection criteria of the samples, and suggested, therefore, that it could not have evolved since $z \sim 0.55$.

The evolution of the KR zero point for cluster galaxies has been investigated in different works in order to perform the Tolman surface brightness test for the universal expansion (Sandage and Perelmuter 1991; Pahre, Djorgovski, and de Carvalho 1996; Sandage and Lubin 2001; Lubin and Sandage 2001a,b,c) and to derive the luminosity evolution of ETGs (e.g. Barger et al. 1998; Ziegler et al. 1999). All these studies concluded that the measured change is consistent with what expected on the basis of cosmological dimming plus passive aging of stellar populations formed at high redshifts.

The KR was investigated at high redshifts for galaxies in the Hubble Deep Field by Fasano et al. (1998), who found that ETGs in the field seem to follow the same restframe KR also at redshifts $z \sim 2-3$.

As shown by La Barbera et al. (2002), it is possible to derive structural parameters of galaxies at intermediate redshifts by using ground–based imaging. In the present work, we use structural parameters in the V-band restframe for a total of $N = 228$ spheroids in the clusters A 209 at z = 0.21, AC 118 at z = 0.31, and EIS 0048−2942 (hereafter EIS 0048) at z = 0.64, and investigate the evolution of the distribution in the $\log \mathrm{r_e}$– $<\mu>_\mathrm{e}$ plane up to a look-back time of ∼ 6 Gyr. Surface photometry for galaxies in A 209, AC 118 and EIS 0048 is published in La Barbera et al. (2003b).

One of the main challenges of previous works on the subject has been represented by selection effects, which can critically affect the determination of the KR. To work out this problem, we introduce a new fitting procedure, which provides un-biased estimates of the KR coefficients, and allows for the first time to investigate the evolution over redshift of the whole distribution in the plane of effective parameters.

The layout of the paper is the following. In Section 2, we present the samples used for the analysis. Section 3 describes the new fitting procedure and deals with the evolution of the KR slope and the comparison of the $\log \mathrm{r_e}$–$<\mu>_\mathrm{e}$ distributions at different redshifts. Section 4 shows the luminosity evolution inferred by the KR. Conclusions are drawn in section 5. In the following, we will assume the cosmology $\Omega_m = 0.3$, $\Omega_\Lambda = 0.7$ and $\mathrm{H_0} = 70\ \mathrm{Kms^{-1}Mpc^{-1}}$. With these parameters, the age of the universe is ∼ 13.5 Gyr, and the redshifts $\mathrm{z} = 0.21, \mathrm{z} = 0.31$, and $\mathrm{z} = 0.64$ correspond to look-back times of $\sim 2.5, 3.5$, and 6 Gyr respectively.

2. The samples

Photometry for the three clusters of galaxies A 209 (z = 0.21), AC 118 (z = 0.31), and EIS 0048 (z = 0.64) resides on data collected at the ESO New Technology Telescope (NTT) and at the ESO Very Large Telescope (VLT). The data relevant for the present study include images in the R band for A 209 and AC 118, and in the I band for EIS 0048, all corresponding approximately to V-band restframe. For AC 118 and EIS 0048, galaxies were selected according to the photometric redshift technique (see Massarotti et al. 2001, and references therein), while for A 209 we considered the sample of spectroscopically confirmed cluster members from Mercurio et al. (2003a) complemented with photometric data (see below). The relevant information on the samples are summarized in table 1.

Structural parameters were derived as described in La Barbera et al. (2002), by fitting galaxy images with Sersic models convolved with suitable representations of the PSF. Uncertainties on structural parameters were estimated as described in La Barbera et al. (2003b), and typically amount to $\delta(\log r_e) \sim 0.09$ and $\delta(<\mu>_e) \sim 0.4$ for A 209, $\delta(\log r_e) \sim 0.14$ and $\delta(<\mu>_e) \sim 0.55$ for AC 118, and to $\delta(\log r_e) \sim 0.07$ and $\delta(<\mu>_e) \sim 0.30$ for EIS 0048. In order to study the KR, we selected the population of spheroids on the basis of the shape of the light profile, as parametrized by the Sersic index n. We classified as spheroids the galaxies with $n > 2$, corresponding to objects with a bulge fraction greater than $\sim 20\%$ (see Saglia et al. 1997; van Dokkum et al. 1998a). For each cluster we considered all the galaxies brighter than a given magnitude limit m_c. Few objects with small radii and poorly determined structural parameters were excluded by selecting only galaxies with $<\mu>_e$ greater than a given surface brightness limit $<\mu>_{e,c}$. The completeness of the spectroscopic sample of A 209 is about 50% at $R \sim 20$, and falls to zero at $R = 21$. A magnitude complete sample was obtained by adding to the spectroscopic data all the spheroids within the colour–magnitude sequence of A 209 (see Mercurio et al. 2003a) down to $R \sim 20.1$. We point out that the present samples constitute the largest data set ($N = 228$) of cluster galaxies, for which the Kormendy relation is investigated up to a look-back time of ~ 6 Gyr.

In order to compare the distributions in the $\log r_e$–$<\mu>_e$ plane at intermediate redshifts with that of nearby galaxies, we took advantage of the large sample of ETGs in the Coma cluster by Jørgensen, Franx, and Kjærgaard (1995a, hereafter JFK95a). Structural parameters for $N = 147$ galaxies were taken in JFK95a, who fitted the growth curve of aperture magnitudes with de Vaucouleurs $r^{1/4}$ profiles and corrected the estimated parameters for seeing effects. The typical uncertainties on $\log r_e$ and $<\mu>_e$ amount to ~ 0.08 and ~ 0.3 mag, respectively (see table 11 of JFK95a). Since it was not possible to select galaxies in the JFK95a sample by using Sersic indices as for the other clusters, we adopted the relation between Sersic index and central velocity dispersion recently found for nearby galaxies by Graham (2002): $\log n \propto \log \sigma_0$. We considered the sample of Coma ETGs with available velocity dispersion from Jørgensen, Franx, and Kjærgaard (1995b, hereafter JFK95b, $N = 76$) and from Jørgensen (1999, hereafter J99, $N = 116$). Among these galaxies, $N = 113$ objects have surface photometry from JFK95a. According to Graham 2002 (Figure 1), we selected galaxies with $\sigma_0 > 110 \ \mathrm{km\,s^{-1}}$, which corresponds to $n \gtrsim 2$, resulting in a sample of $N = 93$ objects. We also excluded from the calculation of the fitting coefficients the three galaxies with largest size in the JFK95a sample: due to the presence of extended halos the use of a de Vaucouleurs model can give very different parameters with respect to the estimates obtained by the Sersic models. The final sample consists in $N = 90$ galaxies brighter than $r_G \sim 15.3$, where r_G is the Thuan–Gunn r-band magnitude [2]. We note that, due to the previous selections, the Coma sample does not constitute a magnitude complete sample of galaxies. This point will be further addressed in Section 3.1.

For A 209, AC 118, and EIS 0048, mean surface brightnesses were corrected for galactic extinction following Schlegel, Finkbeiner, and Davis (1998), while the cosmological dimming

[2] Since spheroids have very small internal colour gradients at optical wavelengths, the difference between the r_G band and the V-band restframe at the Coma redshift is not relevant for the present study

was not removed. For the Coma sample, since both corrections were applied by JFK95a, we added the term $10 \cdot \log(1+z)$ to the $<\mu>_e$ values.

3. Kormendy relations

The $\log R_e$–$<\mu>_e$ diagrams for Coma, A 209, AC 118, and EIS 0048 are shown in Figure 1. For each cluster, spheroids follow a sharp, well defined KR.

3.1. Fitting the KR

Since selection effects can strongly affect the estimate of the KR coefficients (see Ziegler et al. 1999), we fitted the $\log r_e$–$<\mu>_e$ sequences by introducing a modified least square procedure (hereafter MLS, see appendix A), which corrects the bias due to the different completeness cuts in magnitude and $<\mu>_e$ of each sample. The fitting coefficients were derived by minimizing the rms of the residuals with respect to $\log r_e$ and $<\mu>_e$ ($MLS_{\log r_e}$ and $MLS_{<\mu>_e}$ fits), and by applying the bisector regression (BMLS, see Akritas and Bershady 1996), which is more stable and effective with respect to the other fitting methods.

In order to illustrate the reliability of the adopted procedure, we applied different magnitude cuts, R_L, to the sample of AC 118, which has the largest number of galaxies, and for each value of R_L we derived the slope and the zero point of the KR by using the MLS and the ordinary least square (OLS) fits. In Figure 2 we show the variations of β and α as a function of R_L for the bisector fit. Similar results are obtained for the $\log r_e$ and the $<\mu>_e$ regressions. The completeness cut affects significantly the OLS method, producing the well known Malmquist bias: for lower values of R_L the slope of the KR is overestimated while the value of α decreases systematically. On the contrary, it is evident that the MLS procedure removes efficiently the systematic trends of the OLS method, providing un-biased estimates of the KR coefficients. This implies that the MLS fit allows a straightforward comparison of the slope and of the zeropoint of the KR, ruling out any effect related to the different selection criteria of the samples.

Since the selection criteria for the Coma cluster are different with respect to those of the other clusters, we also verified that the fitting results for this sample are not affected by the cuts in magnitude and velocity dispersion. According to the scatter of the relation between velocity dispersion and Sersic index by Graham (2002)[3], we varied the velocity dispersion

[3]We assumed a 2σ dispersion of $\sim 50\,\mathrm{km\,s^{-1}}$

cut within $\pm 25\,\mathrm{km\,s^{-1}}$ and re-derived the MLS coefficients. It turned out that the slope β of the KR changes by few percents, while the corresponding variations of the zeropoint are within ± 0.1mag. These values are fully consistent with the estimates of β and α that are given in Sections 3.2 and 4. A similar result was obtained by changing the magnitude limit of the sample down to $\mathrm{r_g} = 14.5$. It is worth to be noted that the values we obtained for the coefficients of the KR at $\mathrm{z} \sim 0$ are in very good agreement (see Sections 3.2 and 4) with those of previous works for bright nearby ETGs, spanning a much wider luminosity range (see e.g. Capaccioli, Caon, and D'Onofrio 1992). The selection effects on the local reference sample do not affect, therefore, the present analysis.

Another important point is the correlation between the uncertainties on galaxy parameters: for the effective parameters, we have $\delta(\log \mathrm{r_e}) = \gamma \cdot \delta(<\mu>_\mathrm{e})$ (see JFK95a), where the value of γ depends on the methods used to derive $\mathrm{r_e}$ and $<\mu>_\mathrm{e}$, and the corresponding uncertainties. In order to estimate the range of possible values of γ, we compared the uncertainties on $\log \mathrm{r_e}$ and $<\mu>_\mathrm{e}$ for samples of galaxies from different sources (Lucey, Bower, and Ellis 1991; Saglia, Bender, and Dressler 1993; Jørgensen, Franx, and Kjærgaard 1995a; Scodeggio, Giovanelli, and Haynes 1997; Scodeggio, Gavazzi, and Belsole 1998; Mobasher et al. 1999): we found $0.25 \lesssim \gamma \lesssim 0.34$. By using numerical simulations (see La Barbera et al. 2002) and by comparing repeated measurements of $\mathrm{r_e}$ and $<\mu>_\mathrm{e}$ (see La Barbera et al. 2003b), we obtained $\gamma \sim 0.25$ for the parameters of A 209, AC 118, and EIS 0048, in agreement with the quoted range of γ values. The correlation between $\delta(\log \mathrm{r_e})$ and $\delta(<\mu>_\mathrm{e})$ and the typical values of the uncertainties on the effective parameters are shown in Figure 1. The effect on the KR coefficients was estimated by using numerical simulations of the $\log \mathrm{r_e}$–$<\mu>_\mathrm{e}$ diagrams, by a procedure analogous to that described in La Barbera, Busarello, and Capaccioli (2000). We found that the bias on the KR coefficients is negligible, amounting at most to $\sim 3\%$ for AC 118. This is in agreement with what found by Hamabe and Kormendy (1987) for the $\log \mathrm{r_e}$–$<\mu>_\mathrm{e}$ relation of nearby bright ellipticals and spiral bulges.

3.2. Evolution of the slope

The slopes of the KRs are reported in table 2, while the variation of β with redshift is shown in Figure 3. The uncertainties were estimated by the bootstrap method and amount to $\sim$ 4–8% for A 209, AC 118, and EIS 0048. We note that the uncertainty for the Coma sample is significantly higher ($\sim 9 - 12\%$) due to the smaller range of $\log \mathrm{r_e}$. Figure 3 clearly shows that the values of β are fully consistent for each pair of clusters, except for the $\mathrm{MLS}_{\log \mathrm{r_e}}$ and $\mathrm{MLS}_{<\mu>_\mathrm{e}}$ slopes of the Coma sample, which are consistent with the other values at a lower significance level ($\sim 1.5\ \sigma$). This is due to the fact that the $\mathrm{MLS}_{\log \mathrm{r_e}}$ and $\mathrm{MLS}_{<\mu>_\mathrm{e}}$

methods are more sensitive, with respect to the BMLS method, to the range of $\log r_e$ used in the fit[4]. We conclude, therefore, that no significant evolution in the slope of the KR is found up to $z \sim 0.64$. We also note that the weighted means of β reported in table 3 for the various fitting procedures are in very good agreement with values found by previous studies at $z \sim 0$: e.g. $\beta \sim 2.94$ (Hamabe and Kormendy 1987), $\beta = 3.14 \pm 0.09$ (Hoessel, Oegerle, and Schneider 1987) and $2.9 \lesssim \beta \lesssim 3.4$ (Sandage and Lubin 2001).

The evolution of the KR slope with redshift, $\Delta(\beta)$, carries information on the variation in the properties of the mean stellar populations (SPs) as a function of galaxy radius:

$$\Delta(\beta) = \Delta\left(\frac{\mathrm{d}<\mu>_e}{\mathrm{dlog}\, r_e}\right) = \frac{\mathrm{d}\Delta(<\mu>_e)}{\mathrm{dlog}\, r_e} = \frac{\mathrm{dE}}{\mathrm{dlog}\, r_e}, \tag{3}$$

where $E = E(r_e)$ is the luminosity evolution between $z = 0.64$ and $z = 0$ at a given r_e. In appendix B, we use the GISSEL98 synthesis code (Bruzual and Charlot 1993) to derive an approximated analytic expression for E as a function of the age t_f and the metallicity Z of the galaxy SPs. We consider luminosity evolution in the V band, since (1) the filters relative to each sample approximate the V-band restframe and (2) internal colour gradients of spheroids are known to be very small in the optical wavebands and not to evolve significantly at intermediate redshifts (see La Barbera et al. 2003b). For models with formation redshift $z_f \in [1.8, 10]$ and metallicity $Z \in [0.2, 2.5]Z_\odot$, which are suitable to describe the population of spheroids (see also section 4), we show that E depends mainly on t_f, i.e. $E \simeq E(t_f)$, so that Eq. 3 can be approximated as:

$$\Delta(\beta) \simeq \frac{\mathrm{dE}}{\mathrm{dlog}\, t_f} \cdot \frac{\mathrm{dlog}\, t_f}{\mathrm{dlog}\, r_e} = F(t_f) \cdot \frac{\mathrm{dlog}\, t_f}{\mathrm{dlog}\, r_e}, \tag{4}$$

where $F(t_f) = \mathrm{dE}/\mathrm{dlog}\, t_f$ is computed as described in appendix B. Assuming that the maximum allowed variation of β is 2 σ_β (see table 3), we obtain the relation

$$|\, \mathrm{dlog}\, t_f/\mathrm{dlog}\, r_e \,| < 2\sigma_\beta/F(t_f). \tag{5}$$

For a SSP, $F(t_f) \in [1.3, 1.65]$ mag/Gyr, and the value of 2 $\sigma_\beta/F(t_f)$ turns out to be in the range $[0.1, 0.12]$. This implies that the absolute relative variation of t_f per decade of galaxy radius must be smaller than $\sim 28\%$ (~ 0.12 dex). As shown in appendix B, a lower limit is obtained for SP models with a protracted SFR. For an exponential SFR with time scale $\tau = 1$ Gyr, we find $F(t_f) \in [2, 3]$ mag/Gyr and the relative variation of t_f is constrained to be smaller than $\sim 18\%$.

---

[4]In fact, if we include also the three largest galaxies in the fit of the Coma sample, the bisector method gives $\beta = 2.6 \pm 0.4$, that is fully consistent with the value in table 3.

3.3. Evolution of the intrinsic dispersion

Since the values of β are the same at all redshifts, we adopted as common slope in the KR fit the value relative to the BMLS regression, $\beta = 2.92 \pm 0.08$, and computed for each sample the zeropoint α and the scatter $\sigma_{<\mu>_e}$, defined by the rms of the residuals δ in $<\mu>_e$: $\delta = <\mu>_e - \alpha - \beta \cdot \log r_e$. The uncertainties on α and $\sigma_{<\mu>_e}$ were obtained by numerical simulations, taking also into account the measurement error on the adopted value of the slope. We estimated the intrinsic dispersion of the relations ($\sigma^{(i)}_{<\mu>_e}$) by subtracting in quadrature to $\sigma_{<\mu>_e}$ the amount of dispersion on δ due to the measurement errors on $<\mu>_e$ and $\log r_e$. To this aim, we took into account the typical uncertainties on $\log r_e$ and $<\mu>_e$ (see section 2), and their correlation[5]. The values are given in table 4. It is clear from the table that the KR has significant intrinsic dispersion also at intermediate redshifts (~ 0.4 in $<\mu>_e$), and that this dispersion does not change with redshift. The intrinsic dispersion of the KR is consistent with that reported by Hoessel, Oegerle, and Schneider (1987) and Kjærgaard, Jørgensen, and Moles (1993) for nearby galaxies, and is mainly due to neglecting velocity dispersions in the FP relation (Eq. 1).

3.4. Comparison of the distributions of effective parameters

To compare the distributions in the $\log r_e$–$<\mu>_e$ plane, we first shifted the values of $<\mu>_e$ for A 209, AC 118, and EIS 0048 by matching the zeropoints of the KRs, and then applied to each sample the same cuts in magnitude and $<\mu>_e$. Since the MLS fit provides un-biased estimates of the KR coefficients, this procedure is not affected by the different selection criteria of each sample. The Coma cluster was not considered in order to analyze only the samples with structural parameters derived by the same procedure (see below). The combined $\log r_e$–$<\mu>_e$ diagram for A 209, AC 118, and EIS 0048 is shown in Figure 4.

For each cluster, we derived the mean value, $<\log r_e>$, and the standard deviation, $\sigma_{\log r_e}$, of the $\log r_e$ distribution by applying the bi-weight statistics (e.g. Beers et al. 1990), which has the advantage to minimize the effect of outliers. As shown in table 5, the values of $<\log r_e>$ and $\sigma_{\log r_e}$ are fully consistent (within $\sim 1\sigma$) for each pair of clusters[6]. In order

[5]The covariance term between the measurement errors on $\log r_e$ and $<\mu>_e$ was estimated by the same procedure adopted for the typical uncertainties on structural parameters (see section 2). For the Coma cluster, we adopted the covariance term used for EIS 0048, whose structural parameters have similar uncertainties.

[6]This result is not affected by the difference in the measurement uncertainties on r_e among the clusters. In fact, by subtracting in quadrature the error on $\log r_e$ from $\sigma_{\log r_e}$, we obtain the following estimates of the standard deviations: 0.25 ± 0.04, 0.31 ± 0.06 and 0.30 ± 0.08, for A 209, AC 118, and EIS 0048, respectively.

to test the presence of differences in the distributions of effective radii, we also applied the Kolmogorov–Smirnov (KS) test. The probability that the observed samples come from the same parent distribution turned out to be 30% for A 209 and AC 118, 42% for A 209 and EIS 0048, and 35% for AC 118 and EIS 0048, indicating that the distribution of galaxy sizes does not change significantly over the explored redshift interval.

In order to verify the presence of possible differences in the $\log \mathrm{r_e}$–$<\mu>_\mathrm{e}$ diagram among the clusters, we used the two-dimensional KS test (Fasano and Franceschini 1987). The test was repeated by using different shifts for each cluster to take into account the uncertainties on α reported in table 4. Comparing AC 118 with the other two clusters, we found probabilities of the KS statistics between 10% and 25%, while a larger probability ($\sim 50\%$) was obtained by comparing A 209 and EIS 0048. We point out that the last result is of particular interest, since the measurement uncertainties on the parameters of A 209 and EIS 0048 are similar and are comparable with the intrinsic dispersion of the KR. Since the error bars for the AC 118 data are significantly larger, we also performed the KS test by adding further scatter to the $\log \mathrm{r_e}$– $<\mu>_\mathrm{e}$ diagram of A 209 and EIS 0048 in order to mimic the measurement uncertainties on the effective parameters at $z \sim 0.3$. In this case, we obtained higher probabilities, between 50% and 80%, that the sample of AC 118 is drawn from the same parent distribution of the other two clusters.

By considering also the Coma cluster in the comparison of the $\log \mathrm{r_e}$– $<\mu>_\mathrm{e}$ distributions, we obtain $<\log \mathrm{r_e}>= 0.40 \pm 0.03$ and $\sigma_{\log \mathrm{r_e}} = 0.24 \pm 0.03$, while the KS tests for both the one-dimensional and two-dimensional case give probabilities between 5% and 10%. The fact that the KS probabilities and the value of $\sigma_{\log r_e}$ are lower with respect to those obtained for the other distributions can be explained by the different procedure by which the structural parameters of the Coma cluster are derived, and is therefore not relevant for the present analysis.

The previous results, together with those of Sections 3.2 and 3.3, indicate that the distribution in the $\log \mathrm{r_e}$–$<\mu>_\mathrm{e}$ plane for cluster galaxies does not vary significantly at least back to $z \sim 0.64$.

4. Luminosity evolution

The evolution of the zeropoint of the KR over redshift is determined (1) by the variation of the distribution of galaxy sizes and of the KR slope with look-back time, (2) by the effect of the cosmological dimming on $<\mu>_\mathrm{e}$, (3) by the luminosity evolution of galaxy stellar populations, (4) by the values of cosmological parameters. Point (1) is ruled out by the results of Sections 3.2 and 3.4. Since the investigation of point (4) would require a larger number of cluster samples, we will focus the discussion on points (2) and (3).

We start to note that, as for the KR slope, the value of α obtained by the BMLS fit for the Coma sample is consistent with that found by previous studies at z ~ 0. For example, if we adopt the KR slope obtained by Hoessel, Oegerle, and Schneider (1987, hereafter HOS87) in the r band for a sample of 97 bright nearby early–types ($\beta = 3.14$), we obtain $\alpha = 18.60$ for the Coma sample, which is in very good agreement with that of HOS87 reported to our cosmology[7]: $\alpha = 18.55 \pm 0.13$.

Suitable corrections were applied to the data in order to convert the $<\mu>_{\rm e}$ values to the same restframe waveband (V) for each cluster. We used the GISSEL98 synthesis code (Bruzual and Charlot 1993) to construct galaxy templates with different age $\rm t_f$ (referred to $\rm z = 0$), metallicity Z and time scale τ of star formation. In order to consider a wide range of possible spectral types describing the galaxies in our sample, we chose the following range of parameters: $\rm t_f \in [8, 13]$ Gyr, $\rm Z \in [0.5, 1.5] Z_\odot$ and $\tau \in [0.01, 5]$ Gyr. The mean values of the derived corrections and the relative uncertainties are shown in table 6. We notice that the uncertainties are very small ($\lesssim 0.03$ mag), i.e. the dependence on the spectral type is negligible, due to the fact that the observed wavebands approximate closely the V-band restframe for each cluster. We also verified that using SSP spectra by Buzzoni (1989) gives values fully consistent with those of table 6. This proves that it is correct to apply the same corrections to all the galaxies in each cluster. The V-band zeropoints ($<\mu_V>_e$) of the KR were obtained by adding the values reported in table 6 to the values of α (table 4), and the corresponding error budgets were estimated by adding in quadrature the uncertainties on the corrections with σ_α.

In Figure 5 we show the relation between $<\mu_V>_e$ and $\log(1 + \rm z)$. The observed points are well described by a linear relation $<\mu_{\rm V}>_{\rm e} = \Gamma \cdot \log(1 + \rm z)$. A least square fit gives $\Gamma = 7.7 \pm 0.6$, or equivalently: $<\rm I_V>_e \propto (1 + z)^{-3.08 \pm 0.24}$, where $<\rm I_V>_e$ is the mean surface brightness within $\rm r_e$ in linear units. As shown by Lubin and Sandage (2001c), this excludes the relation $<\rm I_V>_e \propto (1 + z)^{-1}$, which would hold in the case of a non-expanding universe. We compare the relation between $<\mu_V>_e$ and $\log(1 + \rm z)$ with a no evolution sequence, that is with a pure Tolman signal $<\rm I_V>_e \propto (1 + z)^{-4}$, and with models that include both cosmological dimming and passive luminosity evolution (see Figure 5). These models were constructed by the GISSEL98 synthesis code as follows. We considered galaxy templates with solar metallicity $\rm Z = Z_\odot$, with different formation redshifts ($\rm z_f = 1, 2, 5, 10$), and

---

[7]We also took into account the k-correction and the cosmological dimming which HOS87 removed from the data.

with two time scales of star formation: $\tau = 1$ Gyr, which gives a suitable description of the evolution of ETG integrated colours, and $\tau = 0.01$ Gyr, which reproduces the properties of a simple stellar population. Changing the value of Z in the range 0.5–1.5$Z_\odot$ does not change significantly the results. The models were arbitrarily scaled to fit the data.

According to what found by previous studies (see Lubin and Sandage 2001c), the trend of $<\mu>_e$ with redshift is well described by the superposition of the Tolman signal with pure (passive) luminosity evolution. The formation redshift of the stellar populations is constrained to be higher than $\mathrm{z_f} \sim 2$ with a confidence level $\gtrsim 2\sigma$, in agreement with what found by previous studies of the KR (Barger et al. 1998 and Ziegler et al. 1999) and of the FP (Kelson et al. 1997; van Dokkum et al. 1998b; Jørgensen 1999; Pahre, Djorgovski, and de Carvalho 2001).

5. Conclusions

We have studied the evolution of the optical, V-band restframe, Kormendy relation in the range $0 \lesssim \mathrm{z} \lesssim 0.64$, by using ground-based effective parameters derived in previous works for the clusters of galaxies A 209 (z = 0.21), AC 118 (z = 0.31), and EIS 0048 (z = 0.64), and published data for the Coma cluster (z $\sim$ 0.023). Galaxies were selected by the photometric redshift technique for AC 118 and EIS 0048 and by spectroscopic redshifts complemented with photometric data for A 209.

We introduce a new fitting procedure, the MLS fit, which provides un-biased estimates of the KR coefficients. This allows, for the first time, to investigate the evolution of the slope and of the scatter of the KR, as well as of the whole distribution in the plane of effective parameters.

The results of the present work can be summarized as follows.

- Spheroids define a tight sequence in the plane of the effective parameters at least back to z $\sim$ 0.64.
- The slope β and the intrinsic dispersion $\sigma^{(\mathrm{i})}_{<\mu>_\mathrm{e}}$ turn out to be consistent at all redshifts. The mean values of β and $\sigma^{(\mathrm{i})}_{<\mu>_\mathrm{e}}$ are 2.92 ± 0.08 and 0.40 ± 0.03, respectively.
- The fact that the KR slopes are the same among all the clusters constrains the possible change in the formation epoch of galaxy stellar populations per decade of radius to be smaller than $\sim 28\%$ for SSP models, and smaller than $\sim 18\%$ for populations having an exponential SFR with $\tau = 1$ Gyr.

- The mean value and the width of the distribution of galaxy sizes are consistent for each pair of clusters. Moreover, the Kolmogorov–Smirnov tests indicate that the whole distribution in the $\log r_e$– $<\mu>_e$ plane do not vary over redshift.

- In agreement with previous studies, the evolution of the KR zeropoint is explained by the superposition of the Tolman signal and the passive evolution of stellar populations with high formation redshift, $z_f > 2$.

These results imply that, whatever the mechanism driving galaxy evolution is, (1) it has already built up the Kormendy relation at $z = 0.64$ and (2) it does not affect significantly the properties of spheroids in the plane of effective parameters from that redshift down to $z \sim 0$. The fact that the KR slope does not evolve with redshift sets constrains on the differential luminosity evolution along the early-type sequence, and, therefore, on the properties of galaxy stellar populations as a function of galaxy radius. These results should be taken into account by any model aimed at reproducing the physical processes underlying formation and evolution of spheroids.

We are grateful to R. de Carvalho and A. Iovino for the helpful discussions. We thank A. Mercurio for providing us with the photometry of the cluster of galaxies A 209. Michele Massarotti is partly supported by a 'MIUR-COFIN' grant.

A. The MLS fits

We consider the statistical model:

$$Y = A + B \cdot X \tag{A1}$$

where X and Y are two random variables describing the distributions of $\log r_e$ and $<\mu>_e$ (or viceversa) and A and B are the zero point and the slope of the KR. In order to derive A and B, we have to take into account the constrains on X and Y arising from the selection cuts. By considering the case of a single cut, we have the following constrain:

$$y < c_1 + c_2 \cdot x \tag{A2}$$

where x and y are the outputs of X and Y, while the coefficients c_1 and c_2 describe the selection cut. The direction of the inequality in Eq. A2 is chosen arbitrarily. In the case of the magnitude limit m_c, with $x = \log r_e$ and $y =<\mu>_e$, we have $c_1 = m_c + 2.5 \cdot \log(2\pi)$ and $c_2 = 5$. This follows from the relation $m_T = -2.5 \cdot \log(2\pi) - 5 \cdot \log r_e + <\mu>_e$, where m_T is the total magnitude, and from the constrain $m_T < m_c$.

For a fixed value of x, the probability to find a point in the interval $(\mathrm{y}, \mathrm{y}+\mathrm{dy})$ is given by

$$\mathrm{P_x(y)dy = K(A, B, c_1, c_2) \cdot \exp\left[-(y - A - B \cdot x)^2/(2\sigma^2)\right] \cdot f(c_1 + c_2 \cdot x - y)dy} \tag{A3}$$

where f is a step function, and the coefficient K is derived by imposing $\int \mathrm{P(y)dy} = 1$. Eq. A3 can be directly generalized to the case of multiple cuts and to a more complex shape of the selection function f. We write the likelihood $L = \prod \mathrm{P_{x_i}(y_i)}$, and derive the coefficients in Eq. A1 by minimizing the function $-\ln L$ with respect to A and B. We notice that in the ordinary least square fit the function f is absent in Eq. A3. Therefore, the term K does not depend on A and B and the minimization of $-\ln L$ reduces to solving a coupled system of linear equations in A and B.

B. Parameterizing the luminosity evolution

Spectra of galaxy templates were constructed by the GISSEL98 synthesis code, considering models with a Scalo IMF and an exponential SFR, $\mathrm{e}^{-\mathrm{t}/\tau}$. We considered SSP spectra and models having a protracted SFR, $\tau = 1.0$ Gyr, with metallicity $\mathrm{Z} = 0.2, 0.4, 1, 2.5\ \mathrm{Z}_\odot$ and age $\mathrm{t_f} \in [4, 13]$ Gyr. The range of $\mathrm{t_f}$ was chosen in order to describe the properties of galaxy templates having formation redshift $\mathrm{z_f} \in [1.8, 10]$ (corresponding to a look-back time $\mathrm{t_{LB}} \in [10, 13]$ Gyr), from $\mathrm{z} = 0.64$ to $\mathrm{z} = 0$.

For both models, we found that the dependence of the V-band magnitude at $z \sim 0$ on $\mathrm{t_f}$ and Z is well described by a second-order polynomial fit:

$$\mathrm{m_V(t_f, Z)} \simeq \sum_{\mathrm{i}=1,2} \mathrm{c_i} \cdot [\log \mathrm{t_f}]^{\mathrm{i}} + \sum_{\mathrm{i}=1,2} \mathrm{d_i} \cdot [\log \mathrm{Z}]^{\mathrm{i}} + \mathrm{cost}, \tag{B1}$$

with a rms of ~ 0.02 mag. The restframe V-band magnitude at $\mathrm{z} = 0.64$ is obtained by substituting $\mathrm{t_f}$ with $\mathrm{t_f} - \mathrm{t_{0.64}}$ in Eq. B1, where $\mathrm{t_{0.64}}$ is the look-back time corresponding to $z = 0.64$. We point out that the presence of cross terms in Eq. B1, such as $\log \mathrm{t_f} \cdot \log \mathrm{Z}$, reduces the rms of the fit only marginally, by less than 0.01 mag, and that, therefore, the luminosity evolution $\mathrm{E} = \mathrm{m_V(t_f - t_{0.64}, Z)} - \mathrm{m_V(t_f, Z)}$ depends mainly on $\mathrm{t_f}$, that is $\mathrm{E} \simeq \mathrm{E(t_f)}$.

The derivative of $\mathrm{E(t_f)}$ with respect to $\mathrm{t_f}$ can be computed analytically from Eq. B1 and is given by the following equation:

$$\mathrm{F(t_f)} = \frac{\mathrm{dE}}{\mathrm{dlog\, t_f}} = \mathrm{c_1} \cdot \left[\frac{\mathrm{t_f}}{\mathrm{t_f} - \mathrm{t_{0.64}}} - 1\right] + 2\mathrm{c_2} \cdot \left[\frac{\mathrm{t_f} \cdot \log(\mathrm{t_f} - \mathrm{t_{0.64}})}{\mathrm{t_f} - \mathrm{t_{0.64}}} - \log \mathrm{t_f}\right]. \tag{B2}$$

This relation was used to compute the range of values of $\mathrm{F(t_f)}$ in section 3.2.

REFERENCES

Akritas, M.G., and Bershady, M.A. 1996, ApJ, 470, 706

Barger, A.J., Aragón-Salamanca, A., Smail, I., Ellis, R.S., Couch, W.J., Dressler, A., Oemler, A., Poggianti, B.M., and Sharples, R.M. 1998, ApJ, 501, 522

Beers, T.C., Flynn, K., and Gebhardt, K. 1990, AJ, 100, 32

Bruzual, G.A., and Charlot, S. 1993, ApJ, 405, 538

Busarello, G., Merluzzi, P., La Barbera, F., Massarotti, M., and Capaccioli, M. 2002, A&A, 389, 787

Buzzoni, A. 1989, ApJS, 71, 817

Capaccioli, M., Caon, N., and D'Onofrio, M. 1992, MNRAS, 259, 323

Capelato, H.V., de Carvalho, R.R., and Carlberg, R.G. 1995, ApJ, 451, 525

Dantas, C.C., Capelato, H.V., Ribeiro, A.L.B., and de Carvalho, R.R. 2003, MNRAS, 340, 398

Fasano, G., Cristiani, S., Arnouts, S., and Filippi, M. 1998, AJ, 115, 1400

Fasano, G., and Franceschini, A. 1987, MNRAS, 225, 155

Graham, A. 2002, MNRAS, 334,859

Graham, A., and Guzmàn, R. 2003, ApJ, in press (astro-ph/0303391)

Hamabe, M., and Kormendy, J. 1987, In: *Structure and Dynamics of Elliptical Galaxies, IAU Symp., No.127*, p.379, ed. de Zeeuw, T., Reidel, Dordrecht.

Hoessel, J.G., Oegerle, W.R., and Schneider, D.P. 1987, AJ, 94, 1111

Jørgensen, I., Franx, M., and Kjærgaard, P. 1995a, MNRAS, 273, 1097

Jørgensen, I., Franx, M., and Kjærgaard, P. 1995b, MNRAS, 276, 1341

Jørgensen, I., Franx, M., and Kjærgaard, P. 1996, MNRAS, 280, 167

Jørgensen, I. 1999, MNRAS, 306, 833, 607

Jørgensen, I., Franx, M., Hjorth, J., and van Dokkum, P. G. 1999, MNRAS, 308, 833

Kauffmann, G. 1996, MNRAS, 281, 487

Kelson, D.D., Illingworth, G.D., van Dokkum, P.G., and Franx, M. 2000, ApJ, 531, 184

Kelson, D.D., van Dokkum, P.G., Franx, M., Illingworth, G.D., and Fabricant, D. 1997, ApJ, 478, 13

Kjærgaard, P., Jørgensen, I., and Moles, M. 1993, ApJ, 418, 617

Kormendy, J. 1977, ApJ, 218, 333

La Barbera, F., Busarello, G., and Capaccioli, M. 2000, A&A, 362, 851

La Barbera, F., Busarello, G., Merluzzi, P., Massarotti, M., and Capaccioli, M. 2002, ApJ, 571, 790

La Barbera, F., Merluzzi, P., Iovino, A., Busarello, G., Massarotti, M., and Capaccioli, M. 2003, A&A, 399, 899

La Barbera, F., Busarello, G., Massarotti, M., Merluzzi, P., and Mercurio, A. 2003, A&A, in press (astro-ph/0211478)

Larson, R.B. 1974, MNRAS, 166, 585

Lubin, L.M., and Sandage, A. 2001, ApJ, 121, 2289

Lubin, L.M., and Sandage, A. 2001, ApJ, 122, 1071

Lubin, L.M., and Sandage, A. 2001, ApJ, 122, 1084

Lucey, J.R., Bower, R.G., and Ellis, R.S. 1991, MNRAS, 249, 755

Massarotti, M., Iovino, A., Buzzoni, A., and Valls-Gabaud, D. 2001, A&A, 380, 425

Mercurio, A., Girardi, M., Boschin, W., Merluzzi, P., and Busarello, G. 2002, A&A, 397, 431

Mercurio, A, Massarotti, M., Merluzzi, P., Girardi, M., Busarello, G., and La Barbera, F. 2003, A&A, submitted (astro-ph/0303598)

Mobasher, B., Guzman, R., Aragon-Salamanca, A., and Zepf, S. 1999, MNRAS, 304, 225

Pahre, M.A., Djorgovski, S.G., and de Carvalho, R.R. 1996, 456, 79

Pahre, M.A., Djorgovski, S.G., De Carvalho, R.R. 2001, Ap&SS, 276, 983

Saglia, R. P., Bender, R., and Dressler, A. 1993, A&A, 279, 75

Saglia, R.P., Bertschinger, E., Baggley, G., Burstein, D., Colless, M., Roger, L.D., McMahan, R.K., Jr., and Wegner, G. 1997, ApJS, 109, 79

Sandage,A., and Lubin, L.M. 2001, ApJ, 121, 2271

Sandage, A., and Perelmuter, J.-M. 1991, ApJ, 370, 455

Schlegel, D.J., Finkbeiner, D.P., and Davis, M. 1998, ApJ, 500, 525

Scodeggio, M., Giovanelli, R., and Haynes, M. P. 1997, AJ, 113, 101

Scodeggio, M., Gavazzi, G., Belsole, E., Pierini, D., and Boselli, A. 1998, MNRAS, 301, 1001

van Dokkum, P.G., Franx, M., Kelson, D.D., Illingworth, G.D., Fisher, D., and Fabricant, D. 1998, ApJ, 500, 714

van Dokkum, P.G., Franx, M., Kelson, D.D., and Illingworth, G.D. 1998, 504, 17

Ziegler, B.L., Saglia, R.P., Bender, R., Belloni, P., Greggio, L., and Seitz, S. 1999, A&A, 346, 13

Table 1. Samples used in the present study. Column 1: cluster identification. Column 2: redshifts. Column 3: waveband. Column 4: sample size. Columns 5, 6: limits in $<\mu>_{\rm e}$ and magnitude. Column 7: references for data reduction and derivation of structural parameters with the following abbreviations: Jørgensen, Franx, and Kjærgaard (1995a,b); Jørgensen (1999); La Barbera et al. (2002); Busarello et al. (2002); La Barbera et al. (2003a,b); Mercurio et al. (2003a,b) (JFK95a,b; J99; LBM02; BML02; LMI03; LBM03; MGB03; MMM03).

	z	Waveband	N	$<\mu>_{\rm e,c}$	mag	Ref.
COMA	0.023	r_g	90	...	15.3	JFK95a, JFK95b, J99
A 209	0.21	R	81	18.6	20.1	MGB03, MMM03, LBM03
AC 118	0.31	R	101	19.1	20.8	BML02, LBM02
EIS 0048	0.64	I	46	18.9	22.0	LMI03, LBM03

Table 2. Slopes of the KR for COMA, A 209, AC 118, and EIS 0048. Columns 2, 3 and 4: values obtained by the different fitting procedures (see text), with the relative uncertainties (1σ standard intervals).

	$\mathrm{MLS}_{\log r_e}$	$\mathrm{MLS}_{<\mu>_e}$	BMLS
COMA	3.9 ± 0.4	2.5 ± 0.3	3.01 ± 0.26
A 209	3.04 ± 0.25	2.70 ± 0.17	2.86 ± 0.17
AC 118	2.84 ± 0.20	2.67 ± 0.15	2.74 ± 0.16
EIS 0048	3.11 ± 0.13	2.97 ± 0.13	3.04 ± 0.13

Table 3. Mean values of the slope β of the KR obtained by the different fitting procedures. The uncertainties σ_β denote 1σ standard intervals.

	β	σ_β
$\mathrm{MLS}_{\log \mathrm{r_e}}$	3.08	0.10
$\mathrm{MLS}_{<\mu>_\mathrm{e}}$	2.78	0.08
BMLS	2.92	0.08

Table 4. Zeropoint and scatter of the KR. Uncertainties denote 1σ standard intervals. $\sigma_{<\mu>_\mathrm{e}}$ is the observed scatter in $<\mu>_\mathrm{e}$, while $\sigma^{(\mathrm{i})}_{<\mu>_\mathrm{e}}$ is the estimate of the intrinsic dispersion of the KR.

	α	$\sigma_{<\mu>_\mathrm{e}}$	$\sigma^{(\mathrm{i})}_{<\mu>_\mathrm{e}}$
COMA	18.68 ± 0.08	0.45 ± 0.05	0.43 ± 0.05
A 209	18.95 ± 0.08	0.51 ± 0.04	0.36 ± 0.07
AC 118	19.45 ± 0.11	0.60 ± 0.05	0.39 ± 0.08
EIS 0048	19.51 ± 0.07	0.42 ± 0.04	0.40 ± 0.04

Table 5. Mean value, $<\log \mathrm{r_e}>$, and standard deviation, $\sigma_{\log \mathrm{r_e}}$, of the $\log \mathrm{r_e}$ distributions. The uncertainties, which indicate 1σ standard intervals, were obtained by the bootstrap method.

	$<\log \mathrm{r_e}>$	$\sigma_{\log \mathrm{r_e}}$
A 209	0.50 ± 0.06	0.27 ± 0.04
AC 118	0.46 ± 0.05	0.34 ± 0.05
EIS 0048	0.48 ± 0.03	0.31 ± 0.08

Table 6. Correction to V-band restframe for the cluster samples. Uncertainties denote 1σ standard intervals.

	COR.
COMA (JFK96)	0.373 ± 0.040
A 209	0.527 ± 0.004
AC 118	0.450 ± 0.020
EIS 0048	1.095 ± 0.030

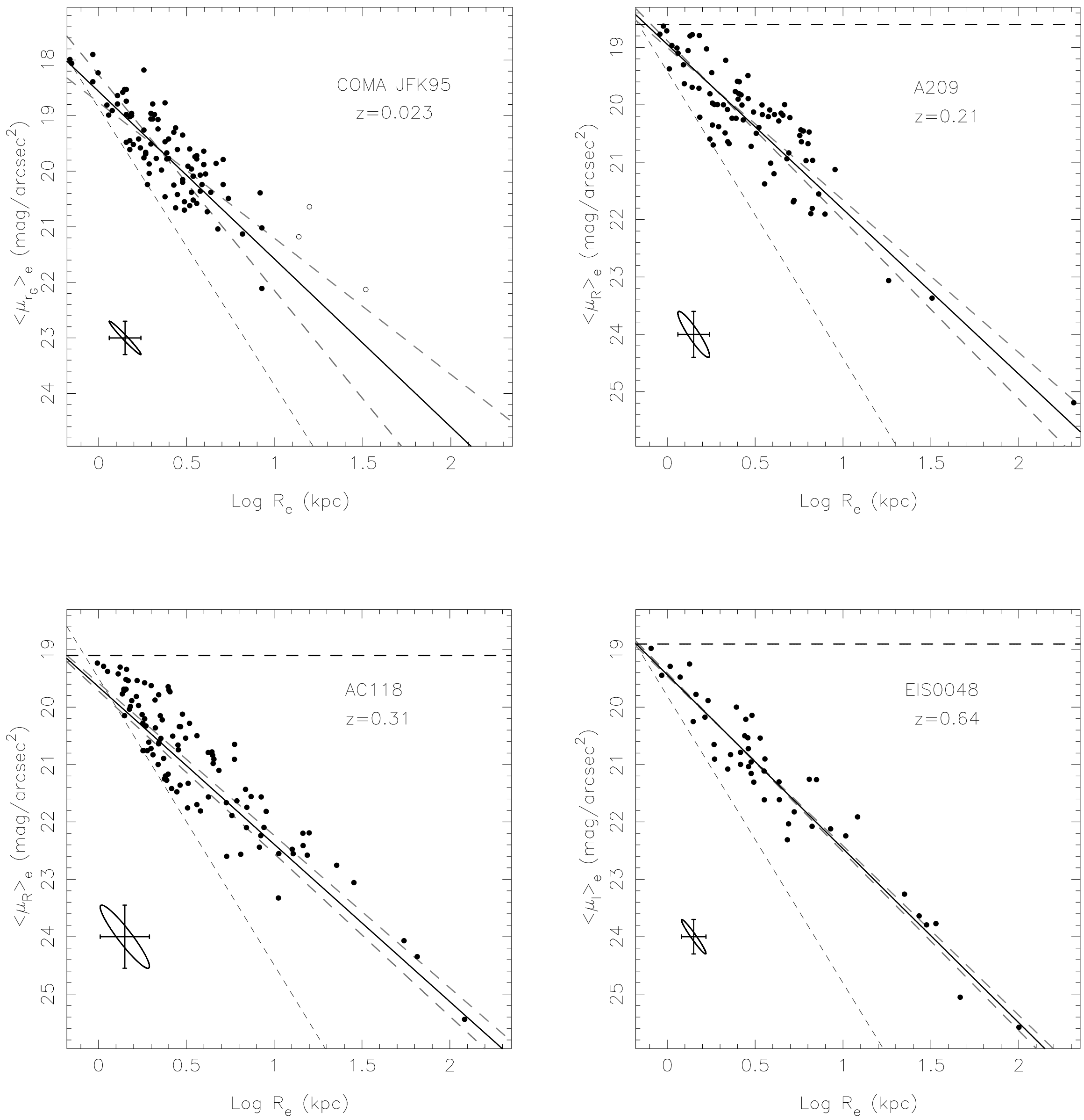

Fig. 1.— Kormendy relations for Coma, A 209, AC 118, and EIS 0048. The range of $\log \mathrm{R_e}$ is the same for each panel, while the range of $<\mu>_\mathrm{e}$ is the same for A 209, AC 118, and EIS 0048, and is shifted by -1 mag arcsec^{-2} for Coma. The $\mathrm{MLS}_{\log \mathrm{r_e}}$ and $\mathrm{MLS}_{<\mu>_\mathrm{e}}$ fits are represented by the long–dashed lines, while the solid line is the BMLS regression. The short–dashed line and the horizontal line indicate the cuts in magnitude and $<\mu>_\mathrm{e}$ for each sample. The correlation of the uncertainties on $\log \mathrm{r_e}$ and $<\mu>_\mathrm{e}$ are shown by the ellipses (1 σ confidence contours) in the lower–right of each panel. The galaxies that were not considered in the fits for the Coma cluster are marked by empty circles.

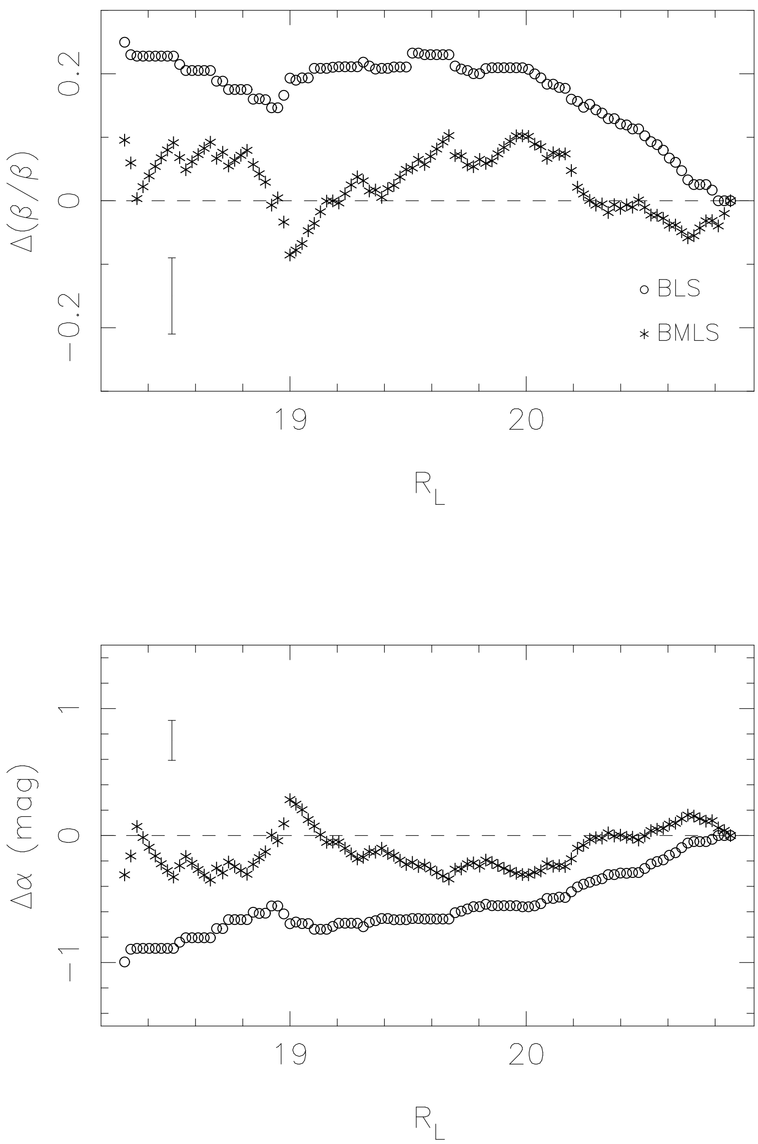

Fig. 2.— Bias on the KR coefficients of AC 118 as a function of the magnitude cut, R_L. Different symbols (see the lower–right corner of the upper panel) denote the bisector ordinary least square (BLS) and the bisector modified least square (BMLS) fits, respectively. In each panel, the mean error bars on the coefficients are shown for reference.

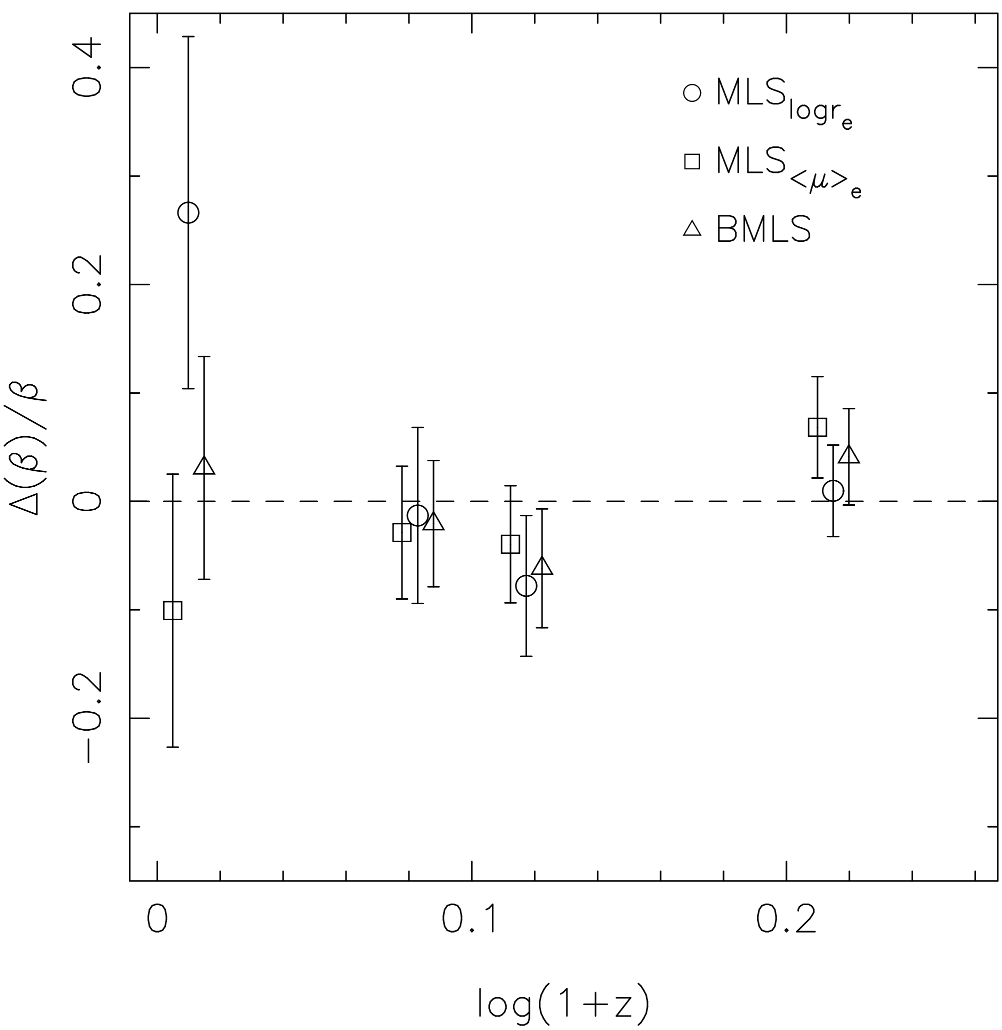

Fig. 3.— Evolution with redshift of the relative slope of the KR. The symbols denote the different fitting methods (see text). For each fitting method, the relative variations were computed with respect to the mean values of table 3.

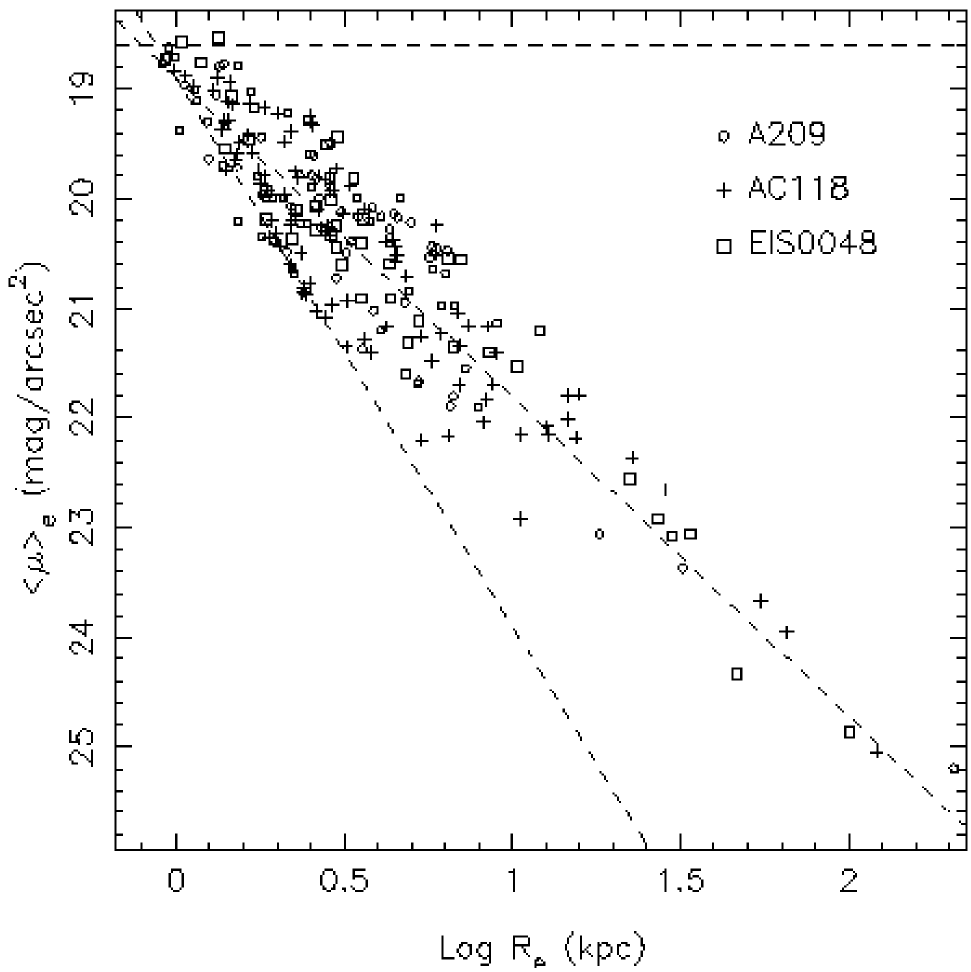

Fig. 4.— Kormendy relations of A 209, AC 118, and EIS 0048, shifted to the same zero point.

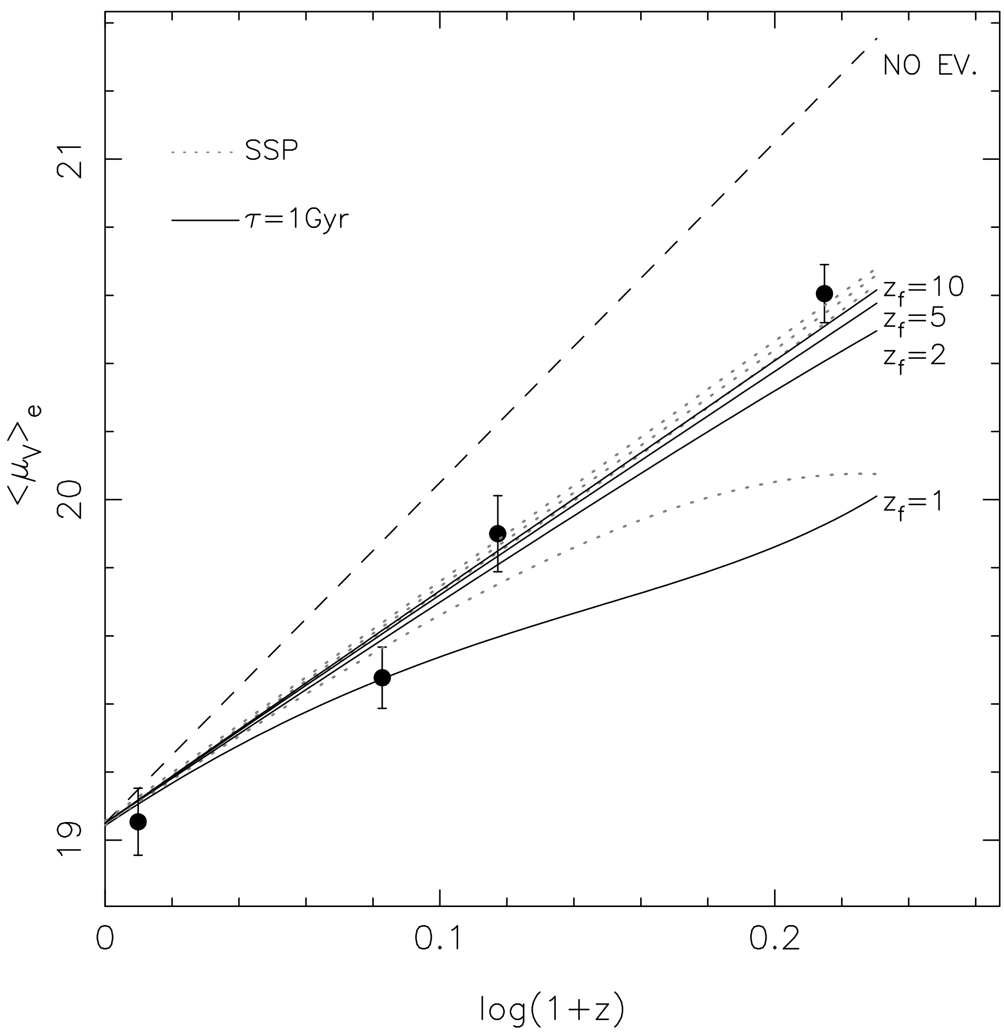

Fig. 5.— Evolution of the zeropoint of the KR. The dashed line indicates the expected change for pure cosmological dimming. The other curves are dimming + passive evolution models corresponding to a SSP with formation redshifts $z_f = 1, 2, 5, 10$ (dotted lines) and to a population with an exponential SFR ($\tau = 1$ Gyr) starting at the redshifts used for the SSP (solid lines).